



Generalized model and performance analysis of two-axis flexure hinges based on quadratic rational Bézier curve

Xuewen Wang, Yang Yu, Zhenbang Xu, Anpeng Xu & Chao Qin

To cite this article: Xuewen Wang, Yang Yu, Zhenbang Xu, Anpeng Xu & Chao Qin (04 Sep 2023): Generalized model and performance analysis of two-axis flexure hinges based on quadratic rational Bézier curve, Mechanics Based Design of Structures and Machines, DOI: [10.1080/15397734.2023.2252508](https://doi.org/10.1080/15397734.2023.2252508)

To link to this article: <https://doi.org/10.1080/15397734.2023.2252508>



Published online: 04 Sep 2023.



Submit your article to this journal [↗](#)



Article views: 53



View related articles [↗](#)



View Crossmark data [↗](#)



Generalized model and performance analysis of two-axis flexure hinges based on quadratic rational Bézier curve

Xuewen Wang^{a,b}, Yang Yu^{a,c}, Zhenbang Xu^{a,b,c}, Anpeng Xu^{a,b}, and Chao Qin^{a,c}

^aChangchun Institute of Optics, Fine Mechanics and Physics, Chinese Academy of Sciences, Changchun, China; ^bUniversity of Chinese Academy of Sciences, Beijing, China; ^cChinese Academy of Science Key Laboratory of On-Orbit Manufacturing and Integration for Space Optics System, Changchun, China

ABSTRACT

This article presents a generalized model of two-axis flexure hinges based on quadratic rational Bézier curve. The generalized closed-form compliance equations are derived based on the virtual work theory and the superposition relationship of the deformation. Then, how to determine the number of sensitive axes, the location of the primary and secondary sensitive axes, and the configuration of the notch profile are discussed. There are 20 types of notch profiles derived from single or mixed, symmetrical or asymmetrical curves. And, the correctness of the compliance equations is verified by finite-element analysis. The maximum relative error does not exceed 10%. Finally, the precision of rotation, the maximum stress, and the effect of structural parameters on the compliance are analyzed. The results show that for two-axis flexure hinges with a flush single curve notch profile, the proximity of the center of rotation to the load end does not significantly affect the axial compliance as well as the torsional compliance. For hybrid two-axis flexure hinges with symmetric structure, the ability to maintain the center of rotation under lateral forces is better than that under the same torque. The proposed generalized model provides a reference for the design of spatial compliant mechanisms.

ARTICLE HISTORY

Received 8 March 2023
Accepted 21 August 2023

KEYWORDS

Bézier curve; compliance; flexure hinge; precision

1. Introduction

Compared to conventional rotating joints, flexure hinges have the advantages of no backlash and no wear, which are widely used in telescopes (Wang et al. 2023; Li, Chen, and Jin 2018), monolithic compliant rotation platforms (Liang et al. 2020), microgrippers (Das et al. 2020), and bridge-lever-type displacement amplifiers (Shen, Zhang, and Qiu 2021; Dong et al. 2018).

The flexure hinge performs the function of rotation by elastic deformation, and the compliance characteristics depend mainly on its notch profile (Ma et al. 2020). To meet the requirements of complex engineering applications, these compliance equations for different notch profiles have been designed and developed one after another. For example, circular flexure hinge (Schotborgh et al. 2005; Yong, Lu, and Handley 2008), elliptical flexure hinge (Chen, Liu, and Du 2011; Chen, Shao, and Huang 2008; Fu et al. 2015), corner-filletted flexure hinge (Lobontiu et al. 2001), parabolic flexure hinge (Chen et al. 2009; Lobontiu, Paine, Garcia, et al. 2002; Lobontiu, Paine, O'Malley, et al. 2002), cycloidal flexure hinge (Tian, Shirinzadeh, and

CONTACT Yang Yu  yuyang@ciomp.ac.cn  Changchun Institute of Optics, Fine Mechanics and Physics, Chinese Academy of Sciences, Changchun, China; Zhenbang Xu  xuzhenbang@ciomp.ac.cn  Changchun Institute of Optics, Fine Mechanics and Physics, Chinese Academy of Sciences, Changchun, China.
Communicated by Francisco J Alonso Sanchez.

Zhang 2010; Tian, Shirinzadeh, and Zhang 2010), power-function-shaped flexure hinge (Li, Pan, and Xu 2013), right-circular corner-filletted flexure hinge (Chen, Jia, and Li 2005a, 2005b), exponent-sine-shaped flexure hinge (Wang, Zhou, and Zhu 2013), etc. It is worth to be noted that Zentner and Linß (2019) have already summarized many flexure hinges with different notch profiles. However, all these compliance equations can still only be applied to design single-axis flexure hinges, as shown in Fig. 1(a). And each compliance equation can be used for only one type of notch profile. Extensive research work has also been carried out to provide more compliance options for the design and optimization of multiple-axis flexure hinges, as shown in Fig. 1(b). Li et al. (2022) have proposed a generalized model and configuration design of multiple-axis flexure hinges under small-deflection occasions. Wang, Wu, and Shao (2021) have derived compliance equations of generalized elliptical-arc-beam spherical flexure hinges based on Castigliano's second theorem. Then, Wei et al. (2021) have derived closed-form compliance equations for elliptic-revolute notch-type multiple-axis flexure hinges based on the beam theory. Finally, Wei et al. (2022) have analyzed closed-form equations of compliance, rotational precision, and maximum stress of hybrid multiple-axis flexure hinges.

In addition, some progress has been made in the research related to two-axis flexure hinges, as shown in Figs. 1(c)–1(e). Lobontiu and Garcia (2003) have proposed a new class of two-axis flexure hinges with axially collocated and symmetric notches based on a parabola. Li et al. (2017) have proposed a generic compliance modeling method for two-axis elliptical-arc-filletted flexure hinges. Wu et al. (2018) have studied two-axis elliptical notch flexure hinge (TENFH) which typically consists of two single-axis elliptical notch flexure hinges. It should be noted that the design of the two-axis flexure hinge needs to be based on the compliance equations of the single-axis flexure hinge. In addition, these investigations mainly focus on elliptical notch profiles. And each compliance equation can be used for only one specific notch profile, which is insufficient for the design and optimization of single-axis and two-axis flexure hinges. To give more compliance options for the design and optimization of spatial compliant mechanisms, a compliance equation applied to both single-axis and two-axis flexure hinges containing more notch profiles needs to be proposed.

The main contribution of this article is the development of a generalized model of two-axis flexure hinges based on quadratic rational Bézier curve. And the generalized closed-form compliance equations in six degrees of freedom based on the virtual work theory and the superposition relationship of the deformation. It is suitable for transverse notch with single axis, compound-transverse notch with two axes, transverse notch with single axis connected in series and parallel. Alternatively, there are 20 types of notch profiles derived from single or mixed, symmetrical, or asymmetrical curves, which can consist of ellipses, circles, hyperbolas, and parabolas. It solves the uniqueness of the determined compliance equation with respect to the notch profile and configuration. Next, how to determine the number of sensitive axes, set up the primary and secondary sensitive axes, and classify the notch profile is discussed in Section 3. And, the correctness of the compliance equation and method is verified by finite element simulation in Section 4. Then, the

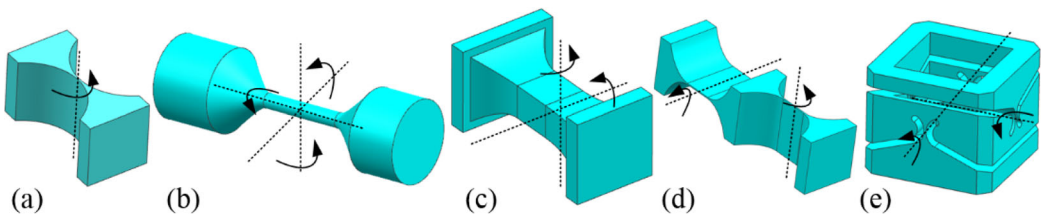


Figure 1. Notch types and sensitive axes of flexure hinges: (a) transverse notch with single axis; (b) revolute notch with multiple axes; (c) compound-transverse notch with two axes; (d) transverse notch with single axis connected in series; (e) transverse notch with single axis connected in parallel.

precision of rotation, the maximum stress, and the effect of structural parameters on the compliance are investigated in Section 5. Finally, some conclusions are given in Section 6.

2. Formulation of the compliance equations

2.1. Two-axis flexure hinges

As shown in Fig. 2, the generalized hybrid two-axis flexure hinge includes segments a , b , c , and d . The lengths of each segment are l_1 , l_2 , l_2 , and l_3 . It should be noted that the thinnest segments b and c are the constant rectangular cross-sectional flexure beam. The dimensions of cross-section A are t_0 and w_0 . The notch profiles of segments a and d are quadratic rational Bézier curves. The dimensions of cross-section B are $t(x)$ and $w(x)$. In addition, the bottom end of the hinge is fixed and the top end is free. In this case, the compliance matrix C of the two-axis flexure hinge can be expressed as (Li et al. 2017)

$$C = \begin{bmatrix} C_{\Delta x-Fx} & 0 & 0 & 0 & 0 & 0 \\ 0 & C_{\Delta y-Fy} & 0 & 0 & 0 & C_{\Delta y-Mz} \\ 0 & 0 & C_{\Delta z-Fz} & 0 & C_{\Delta z-My} & 0 \\ 0 & 0 & 0 & C_{\theta x-Mx} & 0 & 0 \\ 0 & 0 & C_{\theta y-Fz} & 0 & C_{\theta y-My} & 0 \\ 0 & C_{\theta z-Fy} & 0 & 0 & 0 & C_{\theta z-Mz} \end{bmatrix} \quad (1)$$

Next, the compliance matrices of the four segments are defined as C_a , C_b , C_c , and C_d . Then, $O-xyz$ and $O_h-x_hy_hz_h$ are the global and local coordinate systems established at the fixed and free ends, respectively. $O_a-x_a y_a z_a$ (the same for segments b , c , and d) is a local coordinate system established at the tip of segment a . Based on the superposition relation of deformation and the theory of virtual work, the compliance matrix C can be expressed as

$$C = J_a C_a J_a^T + J_b C_b J_b^T + J_c C_c J_c^T + J_d C_d J_d^T \quad (2)$$

where the matrix J_i (the subscript i represents a , b , c , and d .) can be expressed as

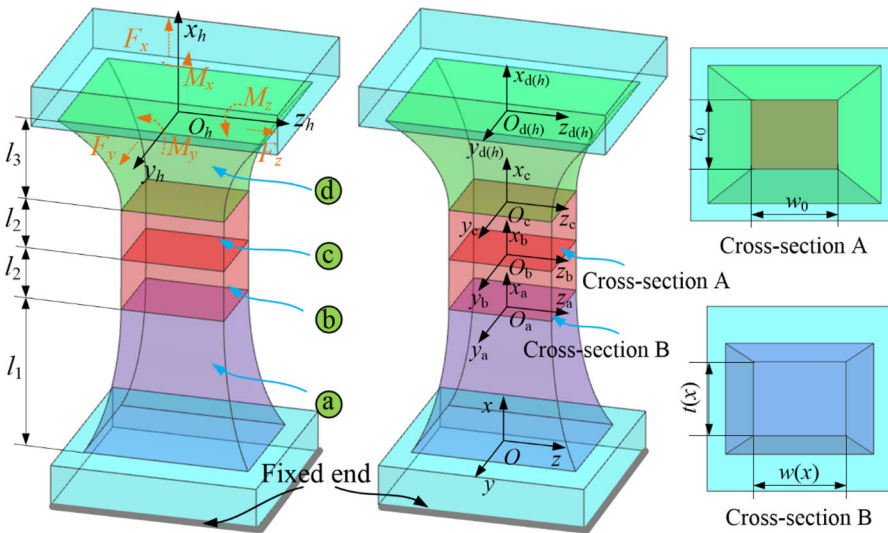


Figure 2. 3D model and geometric parameters of hybrid two-axis flexure hinges.

$$J_i = \begin{bmatrix} \mathbf{R}_i & -\mathbf{R}_i \mathbf{S}_i \\ \mathbf{0}_{3 \times 3} & \mathbf{R}_i \end{bmatrix} \quad (3)$$

where \mathbf{R}_i denotes the attitude of the coordinate system $O_i-x_i y_i z_i$ with respect to the coordinate system $O_h-x_h y_h z_h$. It is remarkable that the unit matrix $\mathbf{R}_i = [1,0,0,0,1,0,0,0,1]$ is the 3×3 square matrix. \mathbf{S}_i can be expressed as

$$\mathbf{S}_i = \begin{bmatrix} 0 & -r_{iz} & r_{iy} \\ r_{iz} & 0 & -r_{ix} \\ -r_{iy} & r_{ix} & 0 \end{bmatrix} \quad (4)$$

in which

$$\mathbf{r}_a = [2l_2 + l_3 \ 0 \ 0], \mathbf{r}_b = [l_2 + l_3 \ 0 \ 0], \mathbf{r}_c = [l_3 \ 0 \ 0], \mathbf{r}_d = [0 \ 0 \ 0] \quad (5)$$

At this point, the compliance matrix \mathbf{C} is converted into solving the compliance matrices \mathbf{C}_a , \mathbf{C}_b , \mathbf{C}_c , and \mathbf{C}_d .

Then, the most important thing is to make the established compliance equations have a wide range of applications. A quadratic rational Bézier curve is used to design the notch profiles of the segments a and d . The advantage is the ability to change the notch profile by controlling the relevant parameters. As shown in Fig. 3, the quadratic rational Bézier curve can be expressed as

$$\begin{bmatrix} x \\ y \end{bmatrix} = \frac{(1-T)^2 \mathbf{P}_0 + 2WT(1-T)\mathbf{P}_1 + T^2 \mathbf{P}_2}{(1-T)^2 + 2WT(1-T) + T^2} \quad (6)$$

where $\mathbf{P}_0 = [x_0, y_0]$, $\mathbf{P}_1 = [x_1, y_1]$ and $\mathbf{P}_2 = [x_2, y_2]$ are the control points, $W \geq 0$ is the weight associated with \mathbf{P}_1 . Then, $T \in [0,1]$, and the shoulder point is $\mathbf{P}_m = [x_m, y_m]$. In addition, the control points and the shoulder point can be expressed as

$$\mathbf{P}_{01} = \frac{\mathbf{P}_0 + W\mathbf{P}_1}{1+W}, \mathbf{P}_{12} = \frac{\mathbf{P}_2 + W\mathbf{P}_1}{1+W}, \mathbf{P}_{02} = \frac{\mathbf{P}_2 + \mathbf{P}_0}{2}, \mathbf{P}_m = \frac{\mathbf{P}_2 + \mathbf{P}_0 + 2W\mathbf{P}_1}{2(1+W)} \quad (7)$$

When $W=0$, the curve is a straight line; When $0 < W < 1$, the curve is an ellipse. When $W=1$, the curve is a parabola. When $W > 1$, the curve is a hyperbola. It is worth noting that the minimum thickness t_0 or w_0 of the hinge is related to y_{\min} . As shown in Figs. 3(a) and 3(b), it is difficult to calculate y_{\min} by T when $y_1 < y_2$ or $y_1 > y_2$. As shown in Fig. 3(c), when $y_1 = y_2$ and $x_1 = (x_0 + x_2)/2$, $y_{\min} = y_m$ (and $T=0.5$) can be derived from Eq. (7). In addition, the relationship between the shoulder point and the control points reveals that the position of the lowest point is related to the weights W , control points \mathbf{P}_0 and \mathbf{P}_2 . Therefore, if segments b and c can be easily determined, the notch profile must be flush. In other words, as shown in Fig. 3(c), the precondition for a flush notch profile is that $y_0 = y_2$.

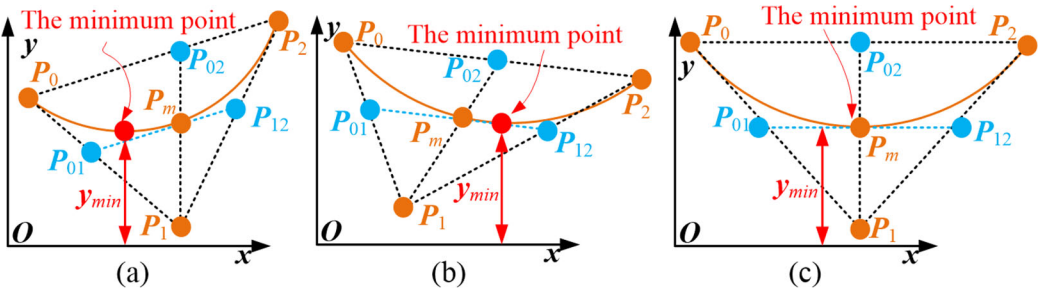


Figure 3. The quadratic rational Bézier curve: (a) $y_0 < y_2$; (b) $y_0 > y_2$; (c) $y_0 = y_2$.

2.2. Compliance equations of segment a

As shown in Fig. 4, $\mathbf{P}_{a1} = [x_{a1}, y_{a1}, z_{a1}]$, $\mathbf{P}_a = [x_a, y_a, z_a]$, and $\mathbf{P}_{a3} = [x_{a3}, y_{a3}, z_{a3}]$ are given as control points of the quadratic rational Bézier curve. Then, the control points are projected onto the planes xoy and xoz to obtain two Bézier curves. W_{ay} and W_{az} are the control weights of the projected points on the planes xoy and xoz , respectively. \mathbf{P}_{a1} and $\mathbf{P}_{a2} = [x_{a2}, y_{a2}, z_{a2}]$ are used as boundary points of the notch profile. The bottom end of segment a is fixed and the top end is free. For better description, the control weights can be expressed as

$$W_{ay} = W_{az} = W_a \quad (8)$$

At this point, the notch profile of segment a can be represented as

$$\begin{bmatrix} x_{ap}(T) \\ y_{ap}(T) \\ z_{ap}(T) \end{bmatrix} = \frac{(1-T)^2 \mathbf{P}_{a1} + 2W_a T(1-T) \mathbf{P}_a + T^2 \mathbf{P}_{a2}}{(1-T)^2 + 2W_a T(1-T) + T^2} \quad (9)$$

Then, according to the analysis in Section 2.1, to make the notch profile flush, some constraints can be expressed as

$$y_{a1} = y_{a3}, z_{a1} = z_{a3}, x_a = x_{a2} = \frac{x_{a1} + x_{a3}}{2} \quad (10)$$

At this moment, $\mathbf{P}_{a2} = [x_{a2}, y_{a2}, z_{a2}]$ can be expressed separately as

$$y_{a2} = y_{ap}(0.5), z_{a2} = z_{ap}(0.5) \quad (11)$$

At this moment, the dimensions $t(x)$ and $w(x)$ of the cross-section B can be expressed separately as

$$t(x) = 2y_{ap}(T), w(x) = 2z_{ap}(T) \quad (12)$$

It is worth noting that the minimum thickness t_0 and w_0 can be expressed as

$$t_0 = 2y_{ap}(0.5) = 2y_{a2}, w_0 = 2z_{ap}(0.5) = 2z_{a2} \quad (13)$$

And then, the cross-section area $A_a(x)$ can be expressed as

$$A_a(x) = t(x)w(x) \quad (14)$$

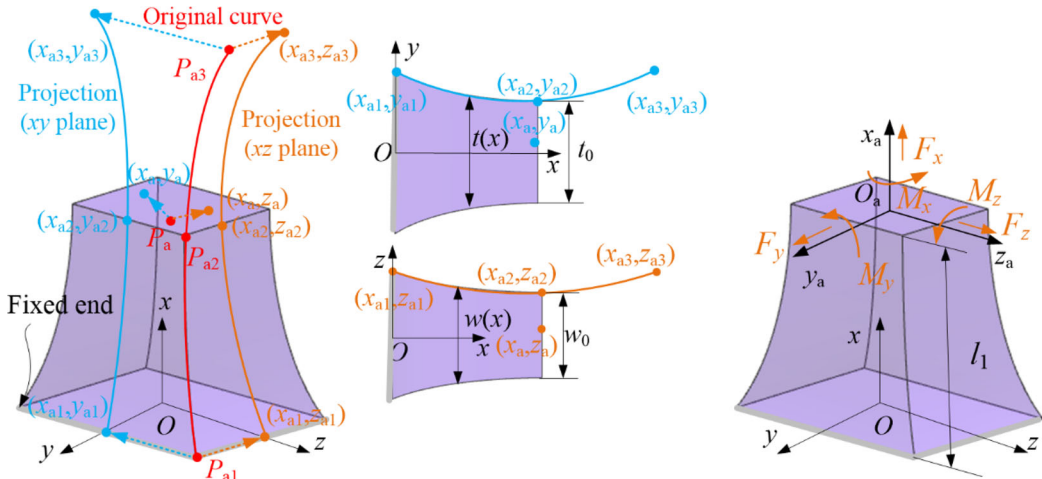


Figure 4. Key geometric parameters of the notch profile and 3D view of segment a .

The second moment of the cross-section area can be expressed as

$$I_{y,a} = \frac{t(x)w^3(x)}{12} = \frac{4y_{ap}(T)z_{ap}^3(T)}{3}, I_{z,a} = \frac{t^3(x)w(x)}{12} = \frac{4y_{ap}^3(T)z_{ap}(T)}{3} \quad (15)$$

Furthermore, the length of the segment a is $l_1 = x_{a2} - x_{a1}$. According to the small deformation assumption, the deformation $\Delta = [\Delta x, \Delta y, \Delta z, \theta x, \theta y, \theta z]$ is related to the external load $F = [Fx, Fy, Fz, Mx, My, Mz]$ can be expressed as

$$\Delta = C_a F \quad (16)$$

It is necessary to note that the compliance is established based on the assumption of small elastic deformation and linearity. C_a is the compliance matrix of segment a , which can be expressed as (Li et al. 2017)

$$C_a = \begin{bmatrix} C_{11,a} & 0 & 0 & 0 & 0 & 0 \\ 0 & C_{22,a} & 0 & 0 & 0 & C_{26,a} \\ 0 & 0 & C_{33,a} & 0 & C_{35,a} & 0 \\ 0 & 0 & 0 & C_{44,a} & 0 & 0 \\ 0 & 0 & C_{53,a} & 0 & C_{55,a} & 0 \\ 0 & C_{62,a} & 0 & 0 & 0 & C_{66,a} \end{bmatrix} \quad (17)$$

Next, C_a is analyzed based on Castigliano's second theorem. And $C_{11,a}$ can be expressed as

$$C_{11,a} = \int_0^{l_1} \frac{dx}{EA_a(x)} = \frac{1}{4E} \int_0^{0.5} \frac{x'_{ap}(T)dT}{y_{ap}(T)z_{ap}(T)} = \frac{1}{4E} N_{1,a} \quad (18)$$

where E is Young's modulus. And $N_{1,a}$ can be expressed as

$$N_{1,a} = \int_0^{0.5} \frac{x'_{ap}(T)dT}{y_{ap}(T)z_{ap}(T)} \quad (19)$$

Second, $C_{22,a}$ can be expressed as

$$\begin{aligned} C_{22,a} &= \int_0^{l_1} \left(\frac{(l_1 - x)^2}{EI_{z,a}} + \frac{\kappa}{GA_a(x)} \right) dx \\ &= \frac{3}{4E} (l_1^2 N_{2,a} - 2l_1 N_{3,a} + N_{4,a}) + \frac{\kappa}{4G} N_{1,a} \end{aligned} \quad (20)$$

where the Poisson ratio is ν , the shear coefficient is $\kappa = (12 + 11\nu)/(10 + 10\nu)$ and G is the shear modulus. In addition, $N_{2,a}$, $N_{3,a}$ and $N_{4,a}$ can be expressed as

$$N_{2,a} = \int_0^{0.5} \frac{x'_{ap}(T)}{y_{ap}^3(T)z_{ap}(T)} dT \quad (21)$$

$$N_{3,a} = \int_0^{0.5} \frac{x_{ap}(T)x'_{ap}(T)}{y_{ap}^3(T)z_{ap}(T)} dT \quad (22)$$

$$N_{4,a} = \int_0^{0.5} \frac{x_{ap}^2(T)x'_{ap}(T)}{y_{ap}^3(T)z_{ap}(T)} dT \quad (23)$$

Third, $C_{33,a}$ can be expressed as

$$\begin{aligned} C_{33,a} &= \int_0^{l_1} \left(\frac{(l_1 - x)^2}{EI_{y,a}} + \frac{\kappa}{GA_a(x)} \right) dx \\ &= \frac{3}{4E} (l_1^2 N_{5,a} - 2l_1 N_{6,a} + N_{7,a}) + \frac{\kappa}{4G} N_{1,a} \end{aligned} \quad (24)$$

where $N_{5,a}$, $N_{6,a}$, and $N_{7,a}$ can be expressed as

$$N_{5,a} = \int_0^{0.5} \frac{x'_{ap}(T)}{y_{ap}(T)z_{ap}^3(T)} dT \quad (25)$$

$$N_{6,a} = \int_0^{0.5} \frac{x_{ap}(T)x'_{ap}(T)}{y_{ap}(T)z_{ap}^3(T)} dT \quad (26)$$

$$N_{7,a} = \int_0^{0.5} \frac{x_{ap}^2(T)x'_{ap}(T)}{y_{ap}(T)z_{ap}^3(T)} dT \quad (27)$$

Fourth, $C_{26,a}$ and $C_{62,a}$ can be expressed as

$$C_{26,a} = C_{62,a} = \int_0^{l_1} \frac{l_1 - x}{EI_{z,a}} dx = \frac{3}{4E} (l_1 N_{2,a} - N_{3,a}) \quad (28)$$

Fifth, $C_{35,a}$ and $C_{53,a}$ can be expressed as

$$C_{35,a} = C_{53,a} = - \int_0^{l_1} \frac{l_1 - x}{EI_{y,a}} dx = - \frac{3}{4E} (l_1 N_{5,a} - N_{6,a}) \quad (29)$$

Then, there are several ways to calculate the torsional compliance of rectangular cross-section beams. However, most of these depend on the relative size of the cross-sectional thickness and width (requiring $w(x)$ to be greater than $t(x)$), which may be changed during the design phase (especially for the optimization of the design). And, the relative size of the thickness and width can affect the accuracy of the calculation (Chen and Howell 2009). To start with, an equation can be expressed as (Lobontiu, Garcia, and Canfield 2004)

$$I_{L,a} = t(x)w^3(x) \left(\frac{1}{3} - 0.21 \frac{w(x)}{t(x)} \right) \quad (30)$$

Then, an approximate equation can be expressed as (Lobontiu, Garcia, and Canfield 2004)

$$I_{YL,a} = t(x)w^3(x) \left(\frac{1}{3} - 0.21 \frac{w(x)}{t(x)} + 0.001 \frac{w^4(x)}{t^4(x)} \right) \quad (31)$$

To neglect the magnitude of $w(x)$ and $t(x)$, Hearn's formula for the polar moment of inertia is used to estimate it (Hearn 1997). The formula can be expressed as

$$I_{H,a} = \frac{t(x)w^3(x)}{3.5 + 3.5w^2(x)/t^2(x)} \quad (32)$$

Then $C_{44,a}$ can be expressed as

$$\begin{aligned} C_{44,a} &= \int_0^{l_1} \frac{dx}{GI_{H,a}} \\ &= \frac{7}{32G} \int_0^{0.5} \frac{x'_{ap}(T) (y_{ap}^2(T) + z_{ap}^2(T)) dT}{y_{ap}^3(T) z_{ap}^3(T)} \\ &= \frac{7}{32G} N_{8,a} \end{aligned} \quad (33)$$

where $N_{8,a}$ can be expressed as

$$N_{8,a} = \int_0^{0.5} \frac{x'_{ap}(T) (y_{ap}^2(T) + z_{ap}^2(T)) dT}{y_{ap}^3(T) z_{ap}^3(T)} \quad (34)$$

Finally, $C_{55,a}$ and $C_{66,a}$ can be expressed as

$$C_{55,a} = \int_0^{l_1} \frac{dx}{EI_{y,a}} = \frac{3}{4E} N_{5,a}, \quad C_{66,a} = \int_0^{l_1} \frac{dx}{EI_{z,a}} = \frac{3}{4E} N_{2,a} \quad (35)$$

2.3. Compliance equations of segments b and c

As shown in Fig. 2, segments b and c are constant rectangular cross-section flexure beams. The cross-sectional dimensions are t_0 and w_0 . The length is l_2 . The compliance matrix $\mathbf{C}_{b(c)}$ can be expressed as

$$\mathbf{C}_{b(c)} = \begin{bmatrix} C_{11,b(c)} & 0 & 0 & 0 & 0 & 0 \\ 0 & C_{22,b(c)} & 0 & 0 & 0 & C_{26,b(c)} \\ 0 & 0 & C_{33,b(c)} & 0 & C_{35,b(c)} & 0 \\ 0 & 0 & 0 & C_{44,b(c)} & 0 & 0 \\ 0 & 0 & C_{53,b(c)} & 0 & C_{55,b(c)} & 0 \\ 0 & C_{62,b(c)} & 0 & 0 & 0 & C_{66,b(c)} \end{bmatrix} \quad (36)$$

The nonzero compliance element of $\mathbf{C}_{b(c)}$ (the subscript $b(c)$ refers to those associated with segments b and c) can be expressed as

$$\begin{cases} C_{11,b(c)} = \frac{l_2}{EA_{b(c)}}, C_{22,b(c)} = \frac{l_2^3}{3EI_{z,b(c)}} + \frac{\kappa l_2}{GA_{b(c)}}, C_{33,b(c)} = \frac{l_2^3}{3EI_{y,b(c)}} + \frac{\kappa l_2}{GA_{b(c)}} \\ C_{26,b(c)} = C_{62,b(c)} = \frac{l_2^2}{2EI_{z,b(c)}}, C_{35,b(c)} = C_{53,b(c)} = -\frac{l_2^2}{2EI_{y,b(c)}} \\ C_{44,b(c)} = \frac{l_2}{GI_{H,b(c)}}, C_{55,b(c)} = \frac{l_2}{EI_{y,b(c)}}, C_{66,b(c)} = \frac{l_2}{EI_{z,b(c)}} \end{cases} \quad (37)$$

It should be noted that the torsional moment $I_{H,b(c)}$ of inertia is adopted from Hearn's formula in order to ignore the magnitude of w_0 and t_0 . The second moment of the cross-section area are $I_{y,b(c)}$ and $I_{z,b(c)}$. And the cross-section area is $A_{b(c)} = t_0 w_0$. At this case, the compliance matrix \mathbf{C} can be determined by simply solving for the compliance matrix of segment d again.

2.4. Compliance equations of segment d

As shown in Fig. 5, $\mathbf{P}_{d1} = [x_{d1}, y_{d1}, z_{d1}]$, $\mathbf{P}_d = [x_d, y_d, z_d]$, and $\mathbf{P}_{d3} = [x_{d3}, y_{d3}, z_{d3}]$ are used as control points of the quadratic rational Bézier curve. According to the analysis in Section 2.2,

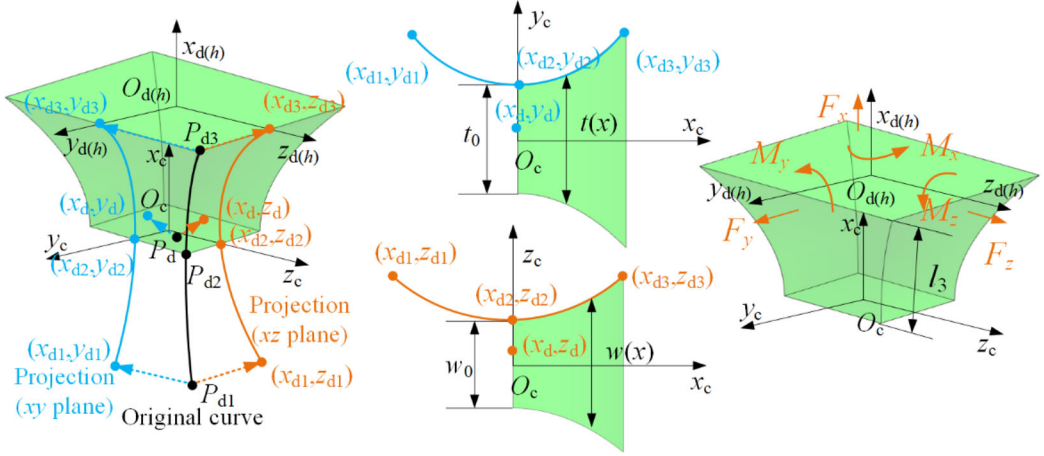


Figure 5. Key geometric parameters of the notch profile and 3D view of segment d .

$W_{dy}=W_{dz}=W_d$. \mathbf{P}_{d1} and $\mathbf{P}_{d2} = [x_{d2}, y_{d2}, z_{d2}]$ are used as boundary points of the notch profile. At this point, this curve can be expressed as

$$\begin{bmatrix} x_{dp}(T) \\ y_{dp}(T) \\ z_{dp}(T) \end{bmatrix} = \frac{(1-T)^2 \mathbf{P}_{d1} + 2W_d T(1-T) \mathbf{P}_d + T^2 \mathbf{P}_{d2}}{(1-T)^2 + 2W_d T(1-T) + T^2} \quad (38)$$

According to the analysis in Section 2.1, some constraints can be expressed as

$$y_{d1} = y_{d3}, z_{d1} = z_{d3}, x_d = x_{d2} = \frac{x_{d1} + x_{d3}}{2} \quad (39)$$

At this moment, $\mathbf{P}_{d2} = [x_{d2}, y_{d2}, z_{d2}]$ can be expressed as

$$y_{d2} = y_{dp}(0.5), z_{d2} = z_{dp}(0.5) \quad (40)$$

Then, the dimensions $t(x)$ and $w(x)$ of the cross-section can be expressed as

$$t(x) = 2y_{dp}(T), w(x) = 2z_{dp}(T) \quad (41)$$

In addition, the minimum thickness t_0 and w_0 can be expressed as

$$t_0 = 2y_{dp}(0.5) = 2y_{d2}, w_0 = 2z_{dp}(0.5) = 2z_{d2} \quad (42)$$

Then, the cross-section area $A_d(x)$ can be expressed as

$$A_d(x) = t(x)w(x) \quad (43)$$

The second moment of the cross-section area can be expressed as

$$I_{yd} = \frac{t(x)w^3(x)}{12} = \frac{4y_{dp}(T)z_{dp}^3(T)}{3}, I_{zd} = \frac{t^3(x)w(x)}{12} = \frac{4y_{dp}^3(T)z_{dp}(T)}{3} \quad (44)$$

Furthermore, the length of the segment d is $l_3=x_d-x_{d1}$. Then, the compliance matrix \mathbf{C}_d of segment d can be expressed as

$$\mathbf{C}_d = \begin{bmatrix} C_{11,d} & 0 & 0 & 0 & 0 & 0 \\ 0 & C_{22,d} & 0 & 0 & 0 & C_{26,d} \\ 0 & 0 & C_{33,d} & 0 & C_{35,d} & 0 \\ 0 & 0 & 0 & C_{44,d} & 0 & 0 \\ 0 & 0 & C_{53,d} & 0 & C_{55,d} & 0 \\ 0 & C_{62,d} & 0 & 0 & 0 & C_{66,d} \end{bmatrix} \quad (45)$$

According to the analysis in [Section 2.2](#), the nonzero compliance element of \mathbf{C}_d can be expressed as

$$C_{11,d} = \frac{1}{4E} N_{1,d} \quad (46)$$

$$C_{22,d} = \frac{3}{4E} (l_3^2 N_{2,d} - 2l_3 N_{3,d} + N_{4,d}) + \frac{\kappa}{4G} N_{1,d} \quad (47)$$

$$C_{44,d} = \frac{7}{32G} N_{8,d} \quad (48)$$

$$C_{33,d} = \frac{3}{4E} (l_3^2 N_{5,d} - 2l_3 N_{6,d} + N_{7,d}) + \frac{\kappa}{4G} N_{1,d} \quad (49)$$

$$C_{26,d} = C_{62,d} = \frac{3}{4E} (l_3 N_{2,d} - N_{3,d}) \quad (50)$$

$$C_{35,d} = C_{53,d} = -\frac{3}{4E} (l_3 N_{5,d} - N_{6,d}) \quad (51)$$

$$C_{55,d} = \frac{3}{4E} N_{5,d} \quad (52)$$

$$C_{66,d} = \frac{3}{4E} N_{2,d} \quad (53)$$

in which

$$N_{1,d} = \int_{0.5}^1 \frac{x'_{dp}(T)}{y_{dp}(T) z_{dp}(T)} dT \quad (54)$$

$$N_{2,d} = \int_{0.5}^1 \frac{x'_{dp}(T)}{y_{dp}^3(T) z_{dp}(T)} dT \quad (55)$$

$$N_{3,d} = \int_{0.5}^1 \frac{x_{dp}(T) x'_{dp}(T)}{y_{dp}^3(T) z_{dp}(T)} dT \quad (56)$$

$$N_{4,d} = \int_{0.5}^1 \frac{x_{dp}^2(T)x'_{dp}(T)}{y_{dp}^3(T)z_{dp}(T)} dT \quad (57)$$

$$N_{5,d} = \int_{0.5}^1 \frac{x'_{dp}(T)}{y_{dp}(T)z_{dp}^3(T)} dT \quad (58)$$

$$N_{6,d} = \int_{0.5}^1 \frac{x_{dp}(T)x'_{dp}(T)}{y_{dp}(T)z_{dp}^3(T)} dT \quad (59)$$

$$N_{7,d} = \int_{0.5}^1 \frac{x_{dp}^2(T)x'_{dp}(T)}{y_{dp}(T)z_{dp}^3(T)} dT \quad (60)$$

$$N_{8,d} = \int_{0.5}^1 \frac{x'_{dp}(T)(y_{dp}^2(T) + z_{dp}^2(T))}{y_{dp}^3(T)z_{dp}^3(T)} dT \quad (61)$$

3. Number of sensitive axes and configuration of notch profiles

In fact, the compliance equation can meet the requirements of more applications, which can provide more compliance options. It is worth emphasizing that the described compliance equations are also capable of deriving a two-axis flexure hinge into a single-axis flexure hinge. If the hinge is a single-axis flexure hinge, the condition of the control weights can be expressed as

$$\begin{cases} W_{ay} = W_{dy} = 0 \\ W_{az} = W_{dz} = 0 \end{cases} \text{ or} \quad (62)$$

In such case, as shown in Fig. 6, the flexure hinge has a transverse notch with single axis. As shown in Figs. 1(d)–1(e), this compliance equations can be used for the design of two-axis flexure hinges in series or parallel, according to the analysis in Section 2. If the above conditions are satisfied, the flexure hinge is a constant rectangular cross-section flexure beam. And if when the above conditions are not satisfied, the flexure hinge has a compound-transverse notch with two axes. In addition, the positions of the primary and secondary sensitive axes are controllable using the control points and control weights.

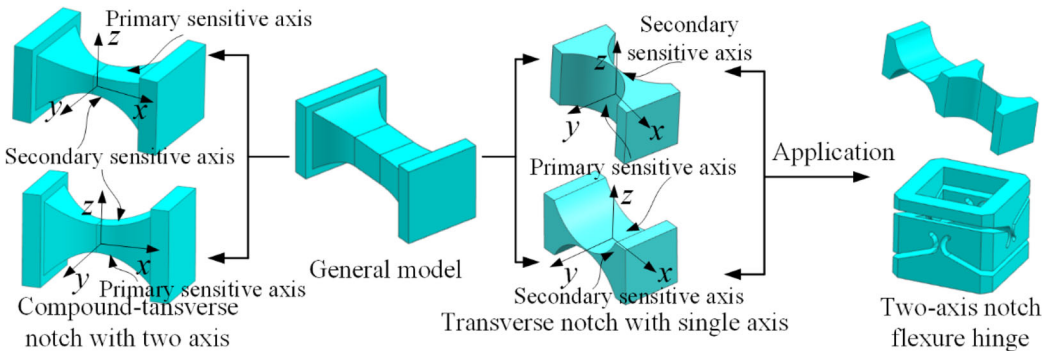


Figure 6. Schematic diagram of the parametric control for hybrid two-axis flexure hinges.

Then, based on the analysis of [Section 2.1](#), the notch profile depends on the control weight W . Thus, the notch profiles of segment a and segment d can be circular, parabolic, elliptical, and hyperbolic. And, the notch profiles can be symmetrical and asymmetrical. In addition, l_2 determines whether the notch profile of the hinge is mixed or single. Thus, there are 20 configurations of notch profiles for two-axis flexure hinges. And, the same is true for single-axis flexure hinges.

To specify the configuration of the notch profile, an analysis based on a binary quadratic implicit equation is proposed. According to the control points $\mathbf{P}_0 = [x_0, y_0]$, $\mathbf{P}_1 = [x_1, y_1]$, $\mathbf{P}_2 = [x_2, y_2]$ and the control weights W in [Section 2.1](#), this equation can be expressed as

$$ax^2 + bxy + cy^2 + dx + ey + f = 0 \quad (63)$$

in which (Anwar, Tasman, and Hariadi 2021)

$$a = y_0^2 - 4W^2y_0y_1 + 4W^2y_1^2 - 2y_0y_2 + 4W^2y_0y_2 - 4W^2y_1y_2 + y_2^2 \quad (64)$$

$$b = -2x_0y_0 + 4W^2x_1y_0 + 2x_2y_0 - 4W^2x_2y_0 + 4W^2x_0y_1 - 8W^2x_1y_1 + 4W^2x_2y_1 + 2x_0y_2 - 4W^2x_0y_2 + 4W^2x_1y_2 - 2x_2y_2 \quad (65)$$

$$c = x_0^2 - 4W^2x_0x_1 + 4W^2x_1^2 - 2x_0x_2 + 4W^2x_0x_2 - 4W^2x_1x_2 + x_2^2 \quad (66)$$

$$d = 4W^2x_1y_1y_2 - 2x_2y_0^2 + 4W^2x_1y_0y_1 + 4W^2x_2y_0y_1 - 4W^2x_0y_1^2 - 4W^2x_2y_1^2 + 2x_0y_0y_2 - 8W^2x_1y_0y_2 + 2x_2y_0y_2 + 4W^2x_0y_1y_2 - 2x_0y_2^2 \quad (67)$$

$$e = 4W^2x_1x_2y_0 - 4W^2x_1^2y_0 + 2x_0x_2y_0 - 2x_2^2y_0 + 4W^2x_0x_1y_1 - 2x_0^2y_2 - 8W^2x_0x_2y_1 + 4W^2x_1x_2y_1 + 4W^2x_0x_1y_2 - 4W^2x_1^2y_2 + 2x_0x_2y_2 \quad (68)$$

$$f = x_2^2y_0^2 - 4W^2x_1x_2y_0y_1 + 4W^2x_0x_2y_1^2 + 4W^2x_1^2y_0y_2 - 2x_0x_2y_0y_2 - 4W^2x_0x_1y_1y_2 + x_0^2y_2^2 \quad (69)$$

According to the analysis in [Section 2](#), the constraints can be expressed as

$$x_1 = \frac{x_0 + x_2}{2}, y_0 = y_2 \quad (70)$$

At this time, the parameters a , b , c , d , e , and f can be expressed as

$$a = 4W^2(y_0 - y_1)^2 \quad (71)$$

$$b = 0 \quad (72)$$

$$c = (1 - W^2)(x_0 - x_2)^2 \quad (73)$$

$$d = 16W^2x_1y_0y_1 - 8W^2x_1(y_1^2 + y_0^2) \quad (74)$$

$$e = 8W^2y_1(x_1^2 - x_0x_2) - 2y_2(x_0 - x_2)^2 \quad (75)$$

$$f = (x_0 - x_2)^2 y_2^2 + 4W^2(x_1^2 y_2^2 + x_0 x_2 y_1^2 - 2x_1^2 y_1 y_2) \quad (76)$$

When $W = 1$ (the curve is parabolic), Eq. (63) can be expressed as

$$ax^2 + dx + ey + f = 0 \quad (77)$$

When $W > 1$ or $0 < W < 1$, Eq. (63) can be expressed as

$$\frac{(y + \frac{e}{2c})^2}{a} + \frac{(x + \frac{d}{2a})^2}{c} = \frac{1}{ac} \left(\frac{d^2}{4a} + \frac{e^2}{4c} - f \right) \quad (78)$$

where $c > 0$, the curve is hyperbolic. Otherwise, the curve is elliptical. Specifically, when the curve is a circle, the constraint can be expressed as

$$W = \sqrt{\frac{(x_0 - x_2)^2}{(x_0 - x_2)^2 + 4(y_0 - y_1)^2}} \quad (79)$$

To better describe the notch profile, some definitions are made. The hybrid-type is abbreviated as H and filleted type is abbreviated as F. Then, the following abbreviations are defined: circular-arc (CA), and elliptical-arc (EA), parabolic-arc (PA), and hyperbolic-arc (HA). At this time, as shown in Fig. 7, the notch profiles are configured as follows: PAPAHF, PAEAHF, PAHAHF, PAPA, PAEAH, PAHAH, EAEAHF, EAHAF, EAEAH, EAHAF, HAHAHF, HAHAH. CACAHF, CACAH, CAEAHF, CAEAH, CAPAHF, CAPAH, CAPAHF, and CAPAH. Therefore, the compliance equations provide more compliance options for the design and optimization of spatial compliant mechanisms.

4. Finite element analysis and validation

Based on the analysis of Section 3, there are 20 configurations for the notch profile of the hinge. It is worth mentioning that circular curve is a special case of elliptical curve, so it is ignored. Therefore, two-axis flexure hinges with 12 notch profiles have been designed to verify the compliance equation. The structural parameters are shown in Table 1. The material of the flexure hinge is structural steel. Young's modulus is 200 GPa, Poisson's ratio is 0.3, and the shear modulus is 76.92 GPa.

The flexure hinge is meshed using PATRAN, as shown in Fig. 8. The element type of the grid is Tet 10. And the element quality needs to be greater than 80%. In addition, the solution type is linear static. One end is fixed and the other end is loaded. To eliminate the additional moment

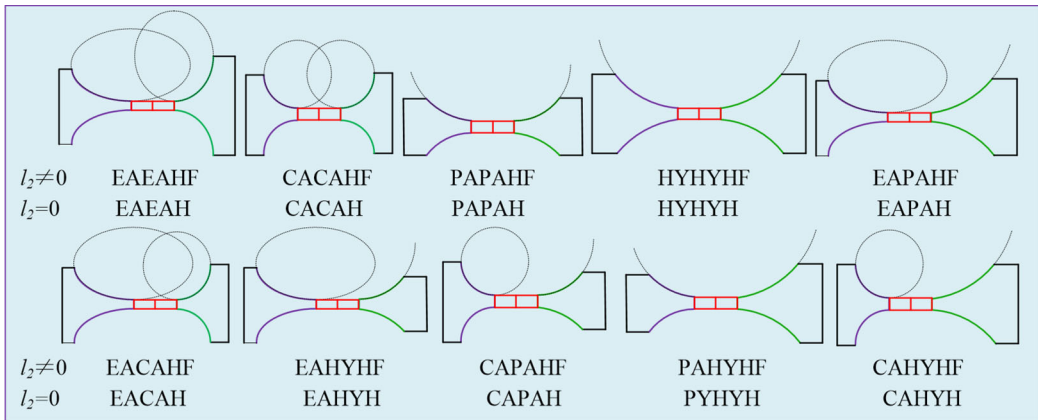
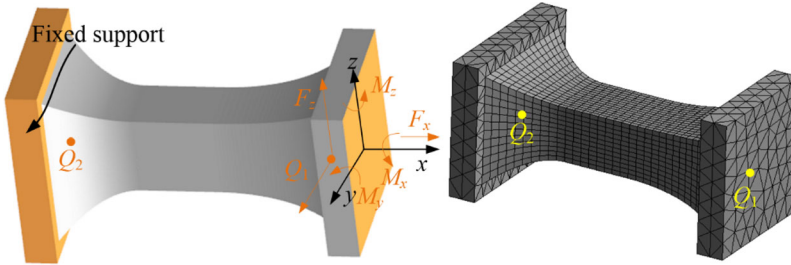


Figure 7. Twenty types of notch profile of the two-axis flexure hinges.

Table 1. Geometric parameters of hybrid two-axis flexure hinges ($x_{a1}=0, x_a=0.5, x_{a3}=1, y_{a1}=-0.7, y_a=0, y_{a3}=0.7$, unit: mm).

No.	y_{a1}, y_a, y_{a3}	z_{a1}, z_a, z_{a3}	W_a	l_2	y_{d1}, y_d, y_{d3}	z_{d1}, z_d, z_{d3}	W_b	type
1	0.5, 0, 0.5	0.4, 0, 0.4	1	0.25	0.5, 0, 0.5	0.4, 0, 0.4	1	PAPAHF
2	0.5, 0, 0.5	0.4, 0, 0.4	1	0.25	0.4, -0.05, 0.4	0.3, 0, 0.3	0.5	PAEAHF
3	0.5, 0, 0.5	0.4, 0, 0.4	1	0.25	0.4, 0.15, 0.4	0.35, 0.1, 0.35	1.5	PAHAHF
4	0.3, -0.1, 0.3	0.4, -0.1, 0.4	1	0	0.3, -0.1, 0.3	0.4, -0.1, 0.4	1	PAPAH
5	0.3, -0.1, 0.3	0.4, -0.1, 0.4	1	0	0.2, -0.1, 0.2	0.2, 0.05, 0.2	0.5	PAEAH
6	0.3, -0.1, 0.3	0.4, -0.1, 0.4	1	0	0.4, -0.1, 0.4	0.3, 0.05, 0.3	1.5	PAHAH
7	0.2, -0.1, 0.2	0.2, 0.05, 0.2	0.5	0.25	0.2, -0.1, 0.2	0.2, 0.05, 0.2	0.5	EAEAHF
8	0.2, -0.1, 0.2	0.2, 0.05, 0.2	0.5	0.25	0.4, -0.1, 0.4	0.3, 0.05, 0.3	1.5	EAAHF
9	0.2, -0.1, 0.2	0.2, 0.05, 0.2	0.5	0	0.2, -0.1, 0.2	0.2, 0.05, 0.2	0.5	EAAH
10	0.2, -0.1, 0.2	0.2, 0.05, 0.2	0.5	0	0.4, -0.1, 0.4	0.3, 0.05, 0.3	1.5	EAAH
11	0.4, -0.1, 0.4	0.3, 0.05, 0.3	1.5	0.25	0.4, -0.1, 0.4	0.3, 0.05, 0.3	1.5	HAHAHF
12	0.4, -0.1, 0.4	0.3, 0.05, 0.3	1.5	0	0.4, -0.1, 0.4	0.3, 0.05, 0.3	1.5	HAHAH

**Figure 8.** Hybrid two-axis flexure hinges: (a) the constraint and load settings; (b) the finite element model.

of lateral force, F_y and F_z are applied on the left surface of the fixed end, and the load in other directions is applied on the right surface of the load end. Then, for segments a and d , the centers Q_1 and Q_2 of the cross-section are selected to measure the linear displacements in each direction. The angular displacement is measured by the rotation of the right surface. The results of the theoretical and finite element analysis are shown in Table 2. The errors in the finite element results are within 10% compared to the theoretical results, which can prove the correctness of the compliance equations and the classification method, as shown in Fig. 9.

5. Characteristics of two-axis flexure hinges

5.1. The center of rotation and the compliance

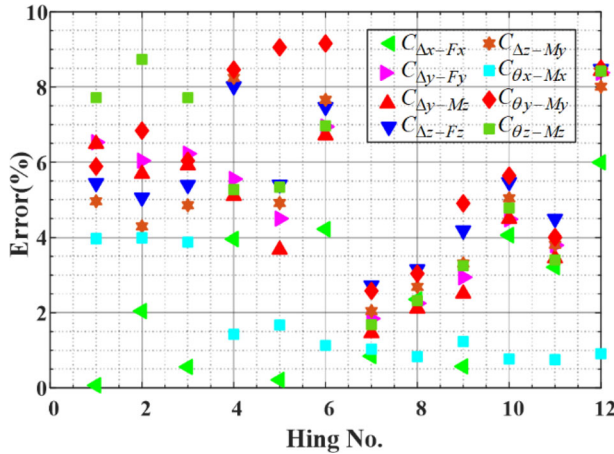
The center of rotation is one of the factors that affect the workspace and performance of precision instruments. One of the characteristics of the established compliance equation is that the position of the center of rotation can be controlled. As shown in Fig. 10, the center Q of rotation of the hinge can be considered as the center at its weakest position. However, the evaluation of the hinge performance based on the center of rotation of the hybrid flexure hinge is very complicated because of the large number of structural parameters. Most importantly, it is very difficult to design hinges based on complex constraints. In addition, the flushness of the notch profile is perhaps the key to the evaluation of the hinge performance. Therefore, the height ratio H_r is defined to describe the degree of flushness of the hinge. the height ratio H_r can be expressed as

$$H_r = \frac{y_{d3}}{y_{a1}} = \frac{z_{d3}}{z_{a1}} \quad (80)$$

When $H_r > 1$ or $H_r < 1$, the notch profile of the hinge is nonflush. When $H_r = 1$, the notch profile is flush. In addition, let $l_2 = 0$, and the necessary constraint can be expressed as

Table 2. Compliance results of the flexure hinge obtained by analytical equations and finite element analysis (denoted by A and F).

No.	C_{11} , mm/N	C_{22} , mm/N	$C_{26(62)}$, rad/N	C_{33} , mm/N	$C_{35(53)}$, rad/N	C_{44} , rad/Nmm	C_{55} , rad/Nmm	C_{66} , rad/Nmm
1(A)	3.18×10^{-5}	1.28×10^{-3}	1.15×10^{-3}	1.95×10^{-3}	-1.79×10^{-3}	2.49×10^{-3}	2.01×10^{-3}	1.28×10^{-3}
1(F)	3.18×10^{-5}	1.36×10^{-3}	1.22×10^{-3}	2.05×10^{-3}	-1.88×10^{-3}	2.59×10^{-3}	2.12×10^{-3}	1.38×10^{-3}
2(A)	3.42×10^{-5}	1.30×10^{-3}	1.19×10^{-3}	1.98×10^{-3}	-1.86×10^{-3}	2.77×10^{-3}	2.23×10^{-3}	1.41×10^{-3}
2(F)	3.35×10^{-5}	1.38×10^{-3}	1.25×10^{-3}	2.08×10^{-3}	-1.94×10^{-3}	2.88×10^{-3}	2.39×10^{-3}	1.54×10^{-3}
3(A)	3.28×10^{-5}	1.29×10^{-3}	1.16×10^{-3}	1.95×10^{-3}	-1.81×10^{-3}	2.58×10^{-3}	2.07×10^{-3}	1.34×10^{-3}
3(F)	3.26×10^{-5}	1.37×10^{-3}	1.23×10^{-3}	2.06×10^{-3}	-1.90×10^{-3}	2.68×10^{-3}	2.19×10^{-3}	1.45×10^{-3}
4(A)	5.22×10^{-5}	5.01×10^{-3}	6.89×10^{-3}	2.41×10^{-3}	-3.19×10^{-3}	1.17×10^{-2}	4.90×10^{-3}	1.06×10^{-2}
4(F)	5.43×10^{-5}	5.29×10^{-3}	7.24×10^{-3}	2.61×10^{-3}	-3.45×10^{-3}	1.19×10^{-2}	5.31×10^{-3}	1.11×10^{-2}
5(A)	6.57×10^{-5}	5.53×10^{-3}	8.08×10^{-3}	2.72×10^{-3}	-3.89×10^{-3}	1.62×10^{-2}	7.21×10^{-3}	1.41×10^{-2}
5(F)	6.55×10^{-5}	5.78×10^{-3}	8.38×10^{-3}	2.87×10^{-3}	-4.08×10^{-3}	1.65×10^{-2}	7.86×10^{-3}	1.49×10^{-2}
6(A)	5.03×10^{-5}	4.78×10^{-3}	6.41×10^{-3}	2.41×10^{-3}	-3.20×10^{-3}	1.09×10^{-2}	4.96×10^{-3}	9.42×10^{-3}
6(F)	5.24×10^{-5}	5.11×10^{-3}	6.84×10^{-3}	2.59×10^{-3}	-3.44×10^{-3}	1.10×10^{-2}	5.42×10^{-3}	1.01×10^{-2}
7(A)	1.17×10^{-4}	2.74×10^{-2}	2.59×10^{-2}	1.38×10^{-2}	-1.26×10^{-2}	3.31×10^{-2}	1.44×10^{-2}	2.92×10^{-2}
7(F)	1.18×10^{-4}	2.79×10^{-2}	2.63×10^{-2}	1.42×10^{-2}	-1.29×10^{-2}	3.34×10^{-2}	1.48×10^{-2}	2.97×10^{-2}
8(A)	1.02×10^{-4}	2.67×10^{-2}	2.42×10^{-2}	1.35×10^{-2}	-1.19×10^{-2}	2.78×10^{-2}	1.22×10^{-2}	2.45×10^{-2}
8(F)	1.04×10^{-4}	2.73×10^{-2}	2.47×10^{-2}	1.40×10^{-2}	-1.23×10^{-2}	2.80×10^{-2}	1.25×10^{-2}	2.51×10^{-2}
9(A)	7.53×10^{-5}	7.96×10^{-3}	1.05×10^{-2}	4.36×10^{-3}	-5.51×10^{-3}	1.94×10^{-2}	8.85×10^{-3}	1.67×10^{-2}
9(F)	7.57×10^{-5}	8.20×10^{-3}	1.08×10^{-2}	4.55×10^{-3}	-5.69×10^{-3}	1.96×10^{-2}	9.29×10^{-3}	1.72×10^{-2}
10(A)	5.99×10^{-5}	7.21×10^{-3}	8.87×10^{-3}	4.05×10^{-3}	-4.82×10^{-3}	1.41×10^{-2}	6.61×10^{-3}	1.20×10^{-2}
10(F)	6.23×10^{-5}	7.53×10^{-3}	9.27×10^{-3}	4.27×10^{-3}	-5.06×10^{-3}	1.42×10^{-2}	6.98×10^{-3}	1.26×10^{-2}
11(A)	9.06×10^{-5}	1.96×10^{-2}	1.93×10^{-3}	9.97×10^{-3}	-9.57×10^{-3}	2.40×10^{-2}	1.06×10^{-2}	2.11×10^{-2}
11(F)	9.35×10^{-5}	2.03×10^{-2}	2.00×10^{-3}	1.04×10^{-2}	-9.93×10^{-3}	2.42×10^{-2}	1.10×10^{-2}	2.18×10^{-2}
12(A)	4.89×10^{-5}	4.12×10^{-3}	5.68×10^{-3}	2.46×10^{-3}	-3.24×10^{-3}	1.03×10^{-2}	5.01×10^{-3}	8.61×10^{-3}
12(F)	5.18×10^{-5}	4.46×10^{-3}	6.16×10^{-3}	2.66×10^{-3}	-3.50×10^{-3}	1.04×10^{-2}	5.43×10^{-3}	9.34×10^{-3}

**Figure 9.** The relative error between the finite element analysis and the analytical results.

$$\begin{cases} W_{az} = W_{ay} = W_{dz} = W_{dy} = W \\ y_{a1} = y_{d1}, y_a = y_d, y_{a3} = y_{d3} \\ z_{a1} = z_{d1}, z_a = z_d, z_{a3} = z_{d3} \end{cases} \quad (81)$$

In addition, the position of the center of rotation can be determined according to Eq. (7). Therefore, it is easy to find that the position of the center of rotation is related to the x -coordinate of the control points P_a and P_d . Therefore, it is prescribed to use $x = x_a = x_d$ to evaluate the performance of the hinge. The effect of the position of the center of rotation on the performance is shown in Fig. 11. When the notch profile is not flush, the compliance of the hinge in all directions decreases as the center of rotation of the hinge approaches the load end. As the height ratio H_r increases, the compliance in all directions is also reduced. It is important to note that when

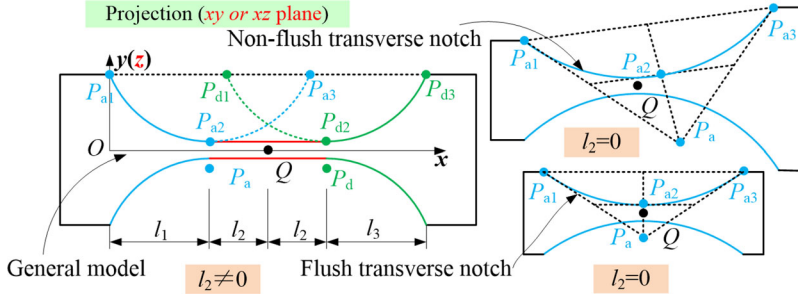


Figure 10. Different configurations of the notch profile and the center of rotation.

the notch profile is flush (i.e., the height ratio is equal to 1), the axial and torsional compliance of the hinge does not change as the center of rotation approaches the load end. In addition, for different notch profiles, the parametric sensitivity of the compliance is from low to high as straight lines, ellipses, parabolas, and hyperbolas. This finding may provide a potential way to increase the workspace of spatial compliant mechanisms during its design and optimization phase.

5.2. Precision of rotation

The precision of rotation is also a relatively important indicator. Here the precision of rotation is analyzed based on a symmetrical structure. On the one hand, the number of control parameters for asymmetric structures is very large. On the other hand, the asymmetry of the notch profile makes the general evaluation approach limited. As shown in Fig. 12, the symmetric reference plane is located between segments b and c . Segments b and c are symmetric about the plane. Segments a and d are also symmetrical. The center of rotation Q lies at the center of the middle cross-section. Then, the compliance matrix C_Q of segments a and b about the center of rotation Q can be expressed as

$$C_Q = \begin{bmatrix} C_{11,Q} & 0 & 0 & 0 & 0 & 0 \\ 0 & C_{22,Q} & 0 & 0 & 0 & C_{26,Q} \\ 0 & 0 & C_{33,Q} & 0 & C_{35,Q} & 0 \\ 0 & 0 & 0 & C_{44,Q} & 0 & 0 \\ 0 & 0 & C_{53,Q} & 0 & C_{55,Q} & 0 \\ 0 & C_{62,Q} & 0 & 0 & 0 & C_{66,Q} \end{bmatrix} \quad (82)$$

In general, the free end of the hinge needs to have a large compliance. However, a smaller off-axis compliance at the center of rotation Q is required to achieve a higher precision of motion. Therefore, the compliance precision ratios are used to evaluate the ability of the free end of the hinge to maintain the center of rotation at the same displacement. Thus, the four compliance precision ratios can be expressed as (Li et al. 2017)

$$R_{22} = \frac{C_{\Delta y - Fy}}{C_{22,Q}}, R_{33} = \frac{C_{\Delta z - Fz}}{C_{33,Q}}, R_{26} = \frac{C_{\theta z - Fy}}{C_{26,Q}}, R_{35} = \frac{C_{\theta y - Fz}}{C_{35,Q}} \quad (83)$$

Then, the compliance matrix C_Q can be expressed as

$$C_Q = J_Q C_a J_Q^T + C_b \quad (84)$$

in which

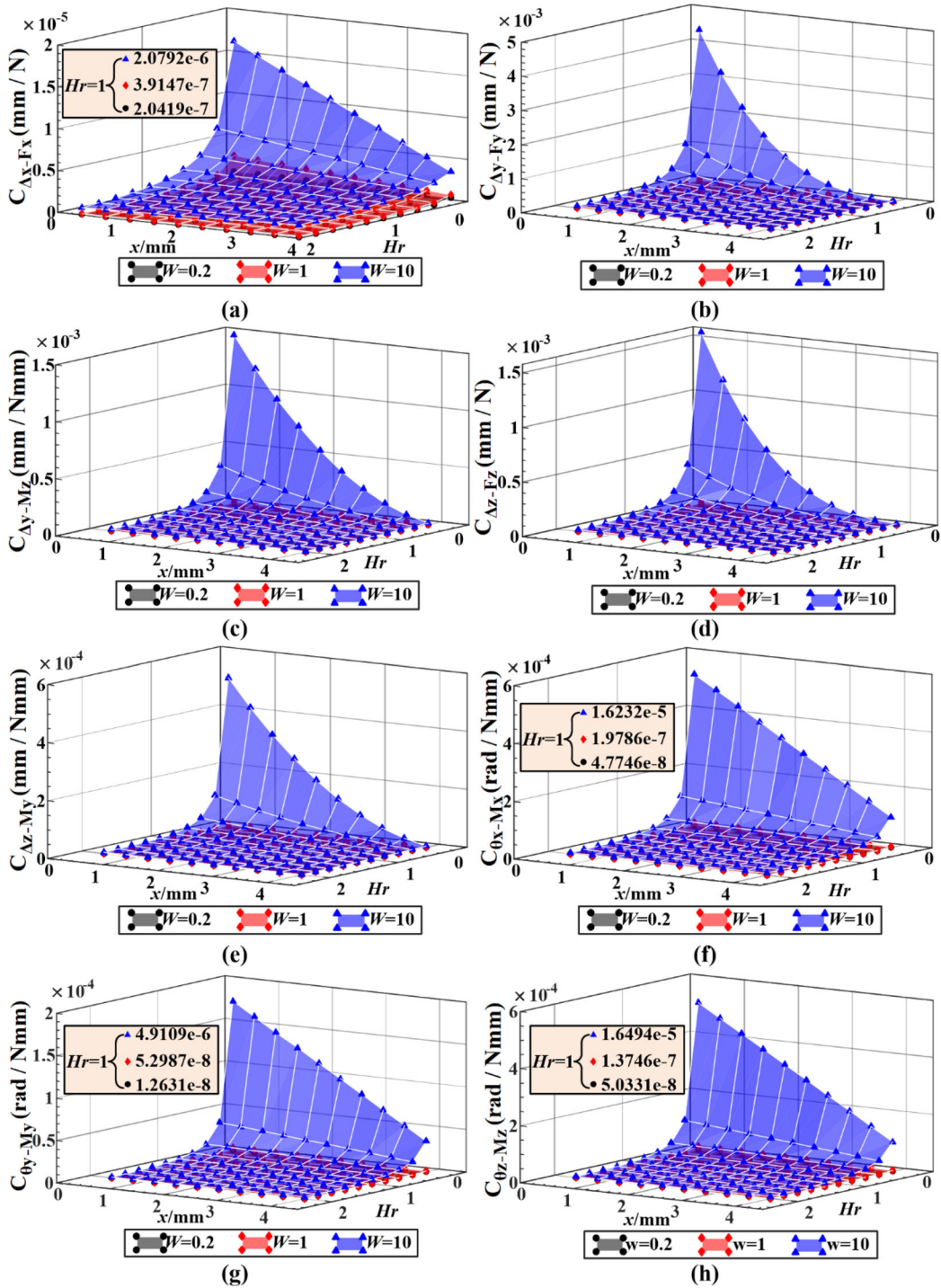


Figure 11. Compliance of hybrid two-axis flexure hinges in multiple directions.

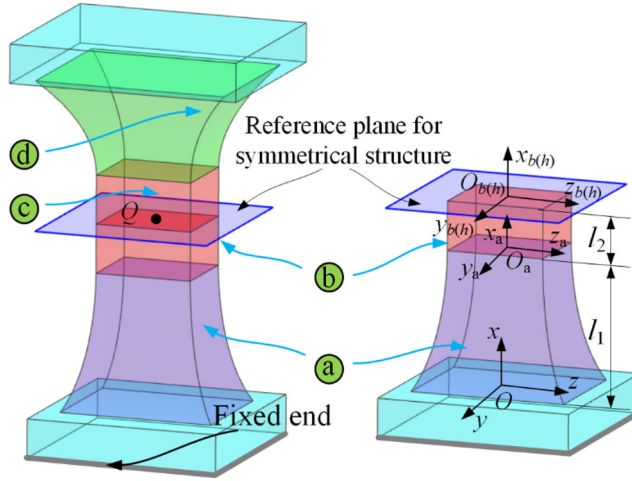


Figure 12. Precision model of hybrid two-axis flexure hinges.

$$J_Q = \begin{bmatrix} \mathbf{R}_Q & -\mathbf{R}_Q \mathbf{S}_Q \\ \mathbf{0}_{3 \times 3} & \mathbf{R}_Q \end{bmatrix} \quad (85)$$

The unit matrix $\mathbf{R}_Q = [1,0,0;0,1,0;0,0,1]$ denotes the attitude of the coordinate system $O_a-x_a y_a z_a$ with respect to the coordinate system $O_b-x_b y_b z_b$. \mathbf{S}_Q can be expressed as

$$\mathbf{S}_Q = \begin{bmatrix} 0 & -r_{Qz} & r_{Qy} \\ r_{Qz} & 0 & -r_{Qx} \\ -r_{Qy} & r_{Qx} & 0 \end{bmatrix} \quad (86)$$

where $\mathbf{r}_Q = [l_2, 0, 0]$.

To quantitatively analyze the compliance precision ratio, the investigation here is mainly based on l_2 and W . On the one hand, the analysis based on other parameters is not beneficial to ensure the structural symmetry of the notch profile. On the other hand, symmetrical structures are very common in the design process of flexure hinges. The trend of the compliance precision ratios is shown in Fig. 13. The compliance precision ratios in all four directions first increase and then decrease as l_2 increases. Then, the compliance precision ratios increase with the increase of W . Moreover, R_{22} and R_{33} are more sensitive to W than R_{26} and R_{35} , respectively. Most importantly, as W and l_2 increase, it is common that R_{22} and R_{33} are greater than R_{26} and R_{35} , respectively. In addition, for different notch profiles, the precision of rotation is from low to high as straight lines, ellipses, parabolas, and hyperbolas, respectively. The analysis results show that the ability of the flexure hinge to maintain the center of rotation under lateral force is better than under the same torque, which provides a theoretical basis for the design and optimization of the spatial compliant mechanism.

5.3. Stress equations

To evaluate the fatigue life of flexure hinges, the stress needs to be explicitly given. When the effects of direct shear and torsion are neglected, the stress of the flexure hinge is mainly dependent on bending and axial effects. Therefore, this stress primarily results from axial forces and moments. In addition, the stress resulting from the axial force is constant, and the stress resulting from the moment is linearly varying. Therefore, the maximum stress of the flexure hinge occurs at the vertex of the cross-section, which is most affected by axial forces and moments, as shown in Fig. 2. The stress σ_{max} can be expressed as (Lobontiu and Garcia 2003)

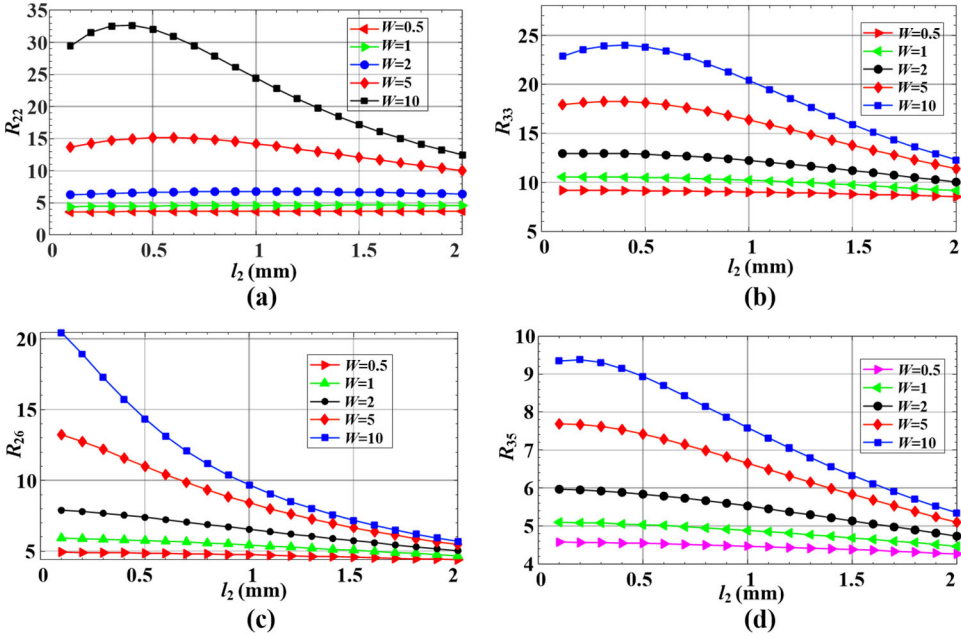


Figure 13. Trend analysis of compliance precision ratios based on parameters.

$$\sigma_{\max} = \frac{1}{w(x)t(x)} \left(K_{t,x} F_x + 6 \left[\frac{K_{t,z}}{t(x)} (F_y L + M_z) + \frac{K_{t,y}}{w(x)} (F_z L + M_y) \right] \right) \quad (87)$$

where $K_{t,x}$, $K_{t,y}$ and $K_{t,z}$ are the stress concentration factors (Chen, Wang, and Liu 2014), the length of the notch profile is $L = l_1 + 2l_2 + l_3$.

In addition, to ensure the fatigue life of the hinge, the maximum stress σ_{\max} should be less than the yield strength σ_s . Further, if the deformation of the flexure hinge needs to be kept linear and elastic, then the maximum stress σ_{\max} should be less than the elastic limit σ_p .

6. Conclusion

In this article, the generalized closed-form compliance equations based on quadratic rational Bézier curve are developed for hybrid two-axis flexure hinges. The equations can be applied to the design and optimization stages of the hinges which can have a transverse notch with single axis, compound-transverse notch with two axes, transverse notch with single axis connected in series or parallel. Alternatively, the notch profile of the hinge can be single and mixed, symmetric and asymmetric curves, which can consist of ellipses, circles, hyperbolas, and parabolas. The established compliance equations are more versatile and concise than the existing compliance equations and provide more compliance options.

Second, it is clearly indicated how to configure the number of sensitive axes and the notch profile. It is beneficial to determine the type of notch profile and the degree of freedom of the hinge according to the requirements of the engineering application. Then, the correctness of the compliance equation and configuration method is further verified by finite element analysis. The results show that the maximum relative error between the analytical results and the finite element analysis does not exceed 10%.

Finally, the effects of structural parameters on the compliance and rotational precision of the hinges are investigated by numerical simulations. The results show that for a two-axis flexure hinge with a flush single curve notch profile, the proximity of the center of rotation to the load

end does not significantly affect the axial compliance as well as the torsional compliance. For flexure hinges with nonflush notch profiles, the compliance in all directions decreases as the center of rotation moves closer to the load end. For the hybrid two-axis flexure hinge with symmetric structure, the compliance precision ratios increase and then decrease in all four directions as l_2 increases. Then the compliance precision ratios increase with the increase of W . Moreover, the sensitivity of R_{22} and R_{33} to W is higher than that of R_{26} and R_{35} , and the ability of the flexure hinge to maintain the center of rotation under lateral forces is better than that under the same torque. In addition, for different notch profiles, the precision of rotation and parametric sensitivity of compliance are from low to high as straight lines, ellipses, parabolas, and hyperbolas, respectively. It is worth being mentioned that the maximum stress is also analyzed and discussed. The relevant theories and conclusions in this article provide theoretical references for the rapid design and optimization of spatial compliant mechanisms.

Data availability

The data that support the findings of this study are available from the corresponding author upon reasonable request.

Disclosure statement

No potential conflict of interest was reported by the authors.

Funding

This work was supported by the National Natural Science Foundation of China (Nos. 11972343 and Nos. 62235018) and Jilin Scientific and Technological Development Program (No. 20220204116YY).

References

- Anwar, Y. R., H. Tasman, and N. Hariadi. 2021. Determining implicit equation of conic section from quadratic rational Bézier curve using Gröbner basis. *Journal of Physics: Conference Series* 2106 (1):012017. doi: [10.1088/1742-6596/2106/1/012017](https://doi.org/10.1088/1742-6596/2106/1/012017).
- Chen, G., and L. L. Howell. 2009. Two general solutions of torsional compliance for variable rectangular cross-section hinges in compliant mechanisms. *Precision Engineering* 33 (3):268–274. doi: [10.1016/j.precisioneng.2008.08.001](https://doi.org/10.1016/j.precisioneng.2008.08.001).
- Chen, G.-M., J.-Y. Jia, and Z.-W. Li. 2005a. Right-circular corner-filletted flexure hinges. IEEE International Conference on Automation Science and Engineering, Edmonton, 01–02 August 2005, 249–253. doi: [10.1109/COASE.2005.1506777](https://doi.org/10.1109/COASE.2005.1506777).
- Chen, G.-M., J.-Y. Jia, and Z.-W. Li. 2005b. On hybrid flexure hinges. Proceedings of the IEEE Networking, Sensing and Control, Tucson, 19–22 March 2005, 700–704. doi: [10.1109/ICNSC.2005.1461275](https://doi.org/10.1109/ICNSC.2005.1461275).
- Chen, G., X. Shao, and X. Huang. 2008. A new generalized model for elliptical arc flexure hinges. *The Review of Scientific Instruments* 79 (9):095103. doi: [10.1063/1.2976756](https://doi.org/10.1063/1.2976756).
- Chen, G., X. Liu, and Y. Du. 2011. Elliptical-arc-fillet flexure hinges: Toward a generalized model for commonly used flexure hinges. *Journal of Mechanical Design* 133 (8):081002. doi: [10.1115/1.4004441](https://doi.org/10.1115/1.4004441).
- Chen, G., X. Liu, H. Gao, and J. Jia. 2009. A generalized model for conic flexure hinges. *The Review of Scientific Instruments* 80 (5):055106. doi: [10.1063/1.3137074](https://doi.org/10.1063/1.3137074).
- Chen, G., J. Wang, and X. Liu. 2014. Generalized equations for estimating stress concentration factors of various notch flexure hinges. *Journal of Mechanical Design* 136 (3):1–8. doi: [10.1115/1.4026265](https://doi.org/10.1115/1.4026265).
- Das, T. K., B. Shirinzadeh, M. Ghafarian, A. Al-Jodah, Y. Zhong, and J. Smith. 2020. Design, analysis and experimental investigations of a high precision flexure-based microgripper for micro/nano manipulation. *Mechatronics* 69:102396. doi: [10.1016/j.mechatronics.2020.102396](https://doi.org/10.1016/j.mechatronics.2020.102396).
- Dong, W., F. Chen, F. Gao, M. Yang, L. Sun, Z. Du, J. Tang, and D. Zhang. 2018. Development and analysis of a bridge-lever-type displacement amplifier based on hybrid flexure hinges. *Precision Engineering* 54:171–181. doi: [10.1016/j.precisioneng.2018.04.017](https://doi.org/10.1016/j.precisioneng.2018.04.017).
- Fu, J., C. Yan, W. Liu, and T. Yuan. 2015. Simplified equations of the compliant matrix for right elliptical flexure hinges. *The Review of Scientific Instruments* 86 (11):115115. doi: [10.1063/1.4936212](https://doi.org/10.1063/1.4936212).

- Hearn, E. J. 1997. *Mechanics of materials: An introduction to the mechanics of elastic and plastic deformation of solids and structural materials*. Amsterdam: Elsevier
- Li, L., D. Zhang, S. Guo, and H. Qu. 2017. A generic compliance modeling method for two-axis elliptical-arc-fillet flexure hinges. *Sensors* 17 (9):2154. doi: [10.3390/s17092154](https://doi.org/10.3390/s17092154).
- Li, L., D. Zhang, H. Qu, and Y. Wang. 2022. Generalized model and configuration design of multiple-axis flexure hinges. *Mechanism and Machine Theory* 169:104677. doi: [10.1016/j.mechmachtheory.2021.104677](https://doi.org/10.1016/j.mechmachtheory.2021.104677).
- Li, Q., C. Pan, and X. Xu. 2013. Closed-form compliance equations for power-function-shaped flexure hinge based on unit-load method. *Precision Engineering* 37 (1):135–145. doi: [10.1016/j.precisioneng.2012.07.010](https://doi.org/10.1016/j.precisioneng.2012.07.010).
- Li, Z., X. Chen, and G. Jin. 2018. Dimensionless design model for biaxial cartwheel flexure hinges. *Mechanics Based Design of Structures and Machines* 46 (4):401–409. doi: [10.1080/15397734.2017.1341841](https://doi.org/10.1080/15397734.2017.1341841).
- Liang, C., F. Wang, Z. Huo, B. Shi, Y. Tian, X. Zhao, and D. Zhang. 2020. A 2-Dof monolithic compliant rotation platform driven by piezoelectric actuators. *IEEE Transactions on Industrial Electronics* 67 (8):6963–6974. doi: [10.1109/TIE.2019.2935933](https://doi.org/10.1109/TIE.2019.2935933).
- Lobontiu, N., and E. Garcia. 2003. Two-axis flexure hinges with axially-located and symmetric notches. *Computers & Structures* 81 (13):1329–1341. doi: [10.1016/S0045-7949\(03\)00056-7](https://doi.org/10.1016/S0045-7949(03)00056-7).
- Lobontiu, N., E. Garcia, and S. Canfield. 2004. Torsional stiffness of several variable rectangular cross-section flexure hinges for macro-scale and mems applications. *Smart Materials and Structures* 13 (1):12–19. doi: [10.1088/0964-1726/13/1/002](https://doi.org/10.1088/0964-1726/13/1/002).
- Lobontiu, N., J. S. N. Paine, E. Garcia, and M. Goldfarb. 2001. Corner-fillet flexure hinges. *Journal of Mechanical Design* 123 (3):346–352. doi: [10.1115/1.1372190](https://doi.org/10.1115/1.1372190).
- Lobontiu, N., J. S. N. Paine, E. Garcia, and M. Goldfarb. 2002. Design of symmetric conic-section flexure hinges based on closed-form compliance equations. *Mechanism and Machine Theory* 37 (5):477–498. doi: [10.1016/S0094-114X\(02\)00002-2](https://doi.org/10.1016/S0094-114X(02)00002-2).
- Lobontiu, N., J. S. N. Paine, E. O'Malley, and M. Samuelson. 2002. Parabolic and hyperbolic flexure hinges: Flexibility, motion precision and stress characterization based on compliance closed-form equations. *Precision Engineering* 26 (2):183–192. doi: [10.1016/S0141-6359\(01\)00108-8](https://doi.org/10.1016/S0141-6359(01)00108-8).
- Ma, W., R. Wang, X. Zhou, and G. Meng. 2020. The performance comparison of typical notched flexure hinges. *Proceedings of the Institution of Mechanical Engineers, Part C: Journal of Mechanical Engineering Science* 234 (9): 1859–1867. doi: [10.1177/0954406219897941](https://doi.org/10.1177/0954406219897941).
- Schotborgh, W. O., F. G. M. Kokkeler, H. Tragter, and F. J. A. M. van Houten. 2005. Dimensionless design graphs for flexure elements and a comparison between three flexure elements. *Precision Engineering* 29 (1):41–47. doi: [10.1016/j.precisioneng.2004.04.003](https://doi.org/10.1016/j.precisioneng.2004.04.003).
- Shen, X., L. Zhang, and D. Qiu. 2021. A lever-bridge combined compliant mechanism for translation amplification. *Precision Engineering* 67:383–392. doi: [10.1016/j.precisioneng.2020.10.010](https://doi.org/10.1016/j.precisioneng.2020.10.010).
- Tian, Y., B. Shirinzadeh, and D. Zhang. 2010. Closed-form compliance equations of filleted V-shaped flexure hinges for compliant mechanism design. *Precision Engineering* 34 (3):408–418. doi: [10.1016/j.precisioneng.2009.10.002](https://doi.org/10.1016/j.precisioneng.2009.10.002).
- Tian, Y., B. Shirinzadeh, D. Zhang, and Y. Zhong. 2010. Three flexure hinges for compliant mechanism designs based on dimensionless graph analysis. *Precision Engineering* 34 (1):92–100. doi: [10.1016/j.precisioneng.2009.03.004](https://doi.org/10.1016/j.precisioneng.2009.03.004).
- Wang, H., S. Wu, and Z. Shao. 2021. Analytical compliance equations of generalized elliptical-arc-beam spherical flexure hinges for 3d elliptical vibration-assisted cutting mechanisms. *Materials* 14 (20):5928. doi: [10.3390/ma14205928](https://doi.org/10.3390/ma14205928).
- Wang, R., X. Zhou, and Z. Zhu. 2013. Development of a novel sort of exponent-sine-shaped flexure hinges. *The Review of Scientific Instruments* 84 (9):095008. doi: [10.1063/1.4821940](https://doi.org/10.1063/1.4821940).
- Wang, X., Y. Yu, Z. Xu, C. Han, J. Sun, and J. Wang. 2023. Design and assessment of a micro-nano positioning hexapod platform with flexure hinges for large aperture telescopes. *Optics Express* 31 (3):3908–3926. doi: [10.1364/OE.476854](https://doi.org/10.1364/OE.476854).
- Wei, H., B. Shirinzadeh, H. Tang, and X. Niu. 2021. Closed-form compliance equations for elliptic-revolute notch type multiple-axis flexure hinges. *Mechanism and Machine Theory* 156:104154. doi: [10.1016/j.mechmachtheory.2020.104154](https://doi.org/10.1016/j.mechmachtheory.2020.104154).
- Wei, H., J. Yang, F. Wu, X. Niu, and B. Shirinzadeh. 2022. Analytical modelling and experiments for hybrid multi-axis flexure hinges. *Precision Engineering* 76:294–304. doi: [10.1016/j.precisioneng.2022.04.004](https://doi.org/10.1016/j.precisioneng.2022.04.004).
- Wu, J., Y. Zhang, Y. Lu, Z. Wen, D. Bin, and J. Tan. 2018. Modeling and design of a two-axis elliptical notch flexure hinge. *The Review of Scientific Instruments* 89 (4):045010. doi: [10.1063/1.5023764](https://doi.org/10.1063/1.5023764).
- Yong, Y. K., T.-F. Lu, and D. C. Handley. 2008. Review of circular flexure hinge design equations and derivation of empirical formulations. *Precision Engineering* 32 (2):63–70. doi: [10.1016/j.precisioneng.2007.05.002](https://doi.org/10.1016/j.precisioneng.2007.05.002).
- Zentner, L., and S. Linß. 2019. Compliant systems. In *Encyclopedia of nanotechnology*, edited by B. Bhushan. Dordrecht: Springer. doi: [10.1515/9783110479744](https://doi.org/10.1515/9783110479744).